CHEMISTRY OF MATERIALS

Article

pubs.acs.org/cm

Generation of Enzymatic Hydrogen Peroxide to Accelerate the Etching of Silver Nanocrystals with Selectivity

Chia-Wei Wang,[†,‡] Xiaojun Sun,[†] Huan-Tsung Chang,[‡,§] and Dong Qin*[,†]

[†]School of Materials Science and Engineering, Georgia Institute of Technology, Atlanta, Georgia 30332, United States

[‡]Department of Chemistry, National Taiwan University, Taipei 106, Taiwan

[§]Department of Chemistry, Chung Yuan Christian University, Chungli District, Taoyuan City, 32023, Taiwan

Supporting Information

ABSTRACT: We report a simple and versatile system for generating highly concentrated H_2O_2 on the surface of nanoparticles through enzymatic oxidation of glucose. It involves immobilization of glucose oxidase, a negatively charged enzyme, on the surface of a positively charged metal nanoparticle via electrostatic attraction. Upon the introduction of glucose at a concentration of 1.7 mM, this system is able to produce enzymatic H_2O_2 on the surface of the nanoparticle, with oxidation power equivalent to that of aqueous H_2O_2 at a concentration of 5 M when it is directly added into the reaction solution. We have evaluated the system for the etching of both twinned and single-crystal Ag nanocubes. We identified that the highly localized and concentrated H_2O_2 generated on the surfaces of Ag twinned cubes would lead to selective etching from the {111} facets parallel to the twin plane, in a fashion identical to the growth process but in the reversed order. For Ag single-crystals nanocubes, the etching would initiate from the corners to gradually transform the cubes into spheres. This study offers the opportunity to control the etching of metal nanocrystals with selectivity for elucidating the mechanism and diversifying the nanocrystals.

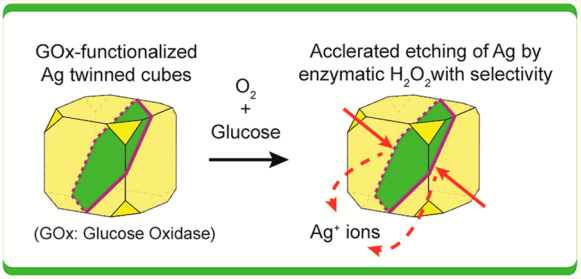

INTRODUCTION

Noble-metal nanocrystals with controlled shapes have received ever increasing attention because of their unique properties for an array of applications in optical sensing,[1−3] biomedical imaging,[4−7] and catalysis.[8−12] A commonly used approach to manipulating the shape of nanocrystals involves seed-mediated growth,[13−16] in which well-defined seeds serve as templates to direct the deposition of atoms. The growth typically progresses more rapidly at sites with higher surface free energies, leading to the formation of nanocrystals enclosed by low-energy facets. Alternatively, oxidative etching has also been explored to maneuver the shape of metal nanocrystals in a controllable fashion.[15,17−21] In this case, the atoms are often oxidized and removed from facets in the order of high to low surface energy, generating nanocrystals with a series of shapes resembling those observed during seed-mediated growth, but in a reserved sequence.[21]

For Ag-based nanocrystals, oxidative etching has been extensively used to transform them into products with new dimensions, compositions, structures, shapes, and morphologies through selective removal of the Ag component.[22] In principle, any chemical with a reduction potential higher than that of Ag^+/Ag can serve as an oxidative etchant. Among them, hydrogen peroxide (H_2O_2) has been well-established as a versatile oxidant due to its easiness of handling.[23] In particular, aqueous H_2O_2 solutions have been extensively used to remove Ag from Ag−M (M = Au, Pd, and Pt) bimetallic nanocrystals for the generation of nanoframes, nanoboxes, and nanocages.[24−29] Despite these successful demonstrations, the use of bulk H_2O_2 has a number of limitations. For example, it relies on a constant supply of H_2O_2 to the surface of a nanocrystal in order to initiate and maintain an etching process, which typically leads to inhomogeneity among different nanocrystals. Additionally, H_2O_2 would become more susceptible to decompose into O_2 in the presence of noble-metal nanoparticles due to their role as a catalyst. As a consequence, it often requires a large excessive amount of H_2O_2 and it also takes a long period of time to complete the etching process. The O_2 bubbles produced from the decomposition of H_2O_2 may also interfere with optical characterization (e.g., *in situ* spectroscopy measurement) and bring challenges to the collection of resultant solids by centrifugation.

One solution to address the aforementioned issues is to generate H_2O_2 *in situ* on the surface of a nanocrystal. It is well-known that glucose oxidase (GOx) can catalyze the oxidation of glucose by O_2 (from air or dissolved in the solution) to produce gluconic acid and H_2O_2.[30] In fact, this reaction has been widely used in the development of new techniques for glucose sensing.[31,32] For example, it has been documented that GOx-functionalized Ag nanoprisms or Ag−Au bimetallic

Received: August 23, 2016
Revised: September 22, 2016
Published: September 30, 2016

DOI: 10.1021/acs.chemmater.6b03546
Chem. Mater. 2016, 28, 7519−7527

nanoparticles could be used for the colorimetric detection of glucose with high sensitivity.[33−35] These studies suggest that the H_2O_2 derived from the enzymatic oxidation of glucose could remove Ag to alter the morphology of nanoparticles, and ultimately change their localized surface plasmon resonance (LSPR) peaks in the visible region. However, to our knowledge, there is no report on a mechanistic understanding of the etching process by enzymatic H_2O_2. In this work, we demonstrate that the highly concentrated H_2O_2 generated on the surface of nanoparticles through enzymatic oxidation of glucose could greatly accelerate the etching process and, at the same time, enable a spatial control. By using Ag twinned cubes as a model system, we demonstrated that the enzymatic H_2O_2 could sequentially remove Ag atoms from the high-energy facets by following a pathway identical to the growth of Ag nanoplates into twinned cubes, but in the reversed order. We also confirmed such selectivity for the etching of single-crystal Ag nanocubes. Collectively, this work suggests that the enzymatic H_2O_2 can serve as an effective means to etch Ag nanocrystals for precisely engineering their shape or morphology to target a variety of applications.

EXPERIMENTAL SECTION

Chemicals and Materials. Ethylene glycol (EG) was purchased from J. T. Baker. All other chemicals were obtained from Sigma-Aldrich and used as received, including silver nitrate ($AgNO_3$, 99+%), silver trifluoroacetate (CF_3COOAg, 98%), gold(III) chloride trihydrate ($HAuCl_4{\cdot}3H_2O$, 99.9+%), ethanol (200 proof), Brilliant Blue G (pure), poly(vinylpyrrolidone) (PVP) with an average molecular weight of 29 000 (PVP−29) or 55 000 (PVP−55), sodium hydrosulfide hydrate ($NaHS{\cdot}xH_2O$), aqueous hydrochloric acid (HCl, 37%), L-ascorbic acid (AA, 99%), sodium hydroxide (NaOH, 98+%), hydrogen peroxide (H_2O_2, 30 wt % in H_2O), cetyltrimethylammonium chloride (CTAC, 98+%), glucose oxidase from *Aspergillus niger* (GOx, 100 000+ units/g), phosphoric acid (H_3PO_4, 85%), phosphoric acid (H_3PO_4, 99+%), sodium phosphate monobasic (NaH_2PO_4, 99+%), sodium phosphate dibasic (Na_2HPO_4, 99+%), sodium phosphate tribasic dodecahydrate ($Na_3PO_4{\cdot}12H_2O$, 98+%), and glucose (99.5+%). All aqueous solutions were prepared using deionized (DI) water with a resistivity of 18.2 MΩ·cm.

Synthesis of Ag Nanoplates, Twinned Cubes, Single-Crystal Cubes. We followed our published protocols for the synthesis of Ag nanoplates,[36] twinned cubes,[37] and single-crystal cubes,[38] respectively. For the synthesis of Ag nanoplates, the product was collected by centrifugation at a speed of 15 000 rpm, washed twice with ethanol, and then redispersed in 0.5 mL of DI water for future use. For the synthesis of Ag twinned cubes, the product was collected by centrifugation at 5000 rpm, washed with DI water, and finally redispersed in 6.1 mL of DI water for future use. For the synthesis of Ag single-crystal cubes, after centrifugation and washing with acetone and DI water three times, the Ag nanocubes were dispersed and stored in 7.2 mL of DI water.

Preparation of CTAC-Functionalized Twinned Cubes. In a typical process, 0.1 mL of CTAC (10 mM) and 0.5 mL of DI water were mixed in a 1.5 mL plastic vial, followed by the addition of 0.4 mL of the twinned cubes. After 30 min, the solids were collected by centrifugation at 5000 rpm and then redispersed in 1.0 mL of DI water for future use.

Preparation of GOx-Functionalized Twinned Cubes. In a typical process, 1 mL of CTAC-functionalized twinned cubes was injected to a 1.5 mL plastic vial, followed by the injection of 10 μL of GOx solution (1000 units/mL). After 5 min, the solids and supernatant were collected by centrifugation at 15 000 rpm for the etching process and the quantification of GOx, respectively.

Preparation of Bradford Reagent. 1 mg of Brilliant Blue G was dissolved in 0.5 mL of ethanol, followed by the addition of 1 mL of phosphoric acid (85%). The solution was further diluted to 10 mL with DI water and filtered twice through filter paper.

Bradford Assay. 0−40 μL of GOx solutions (100 units/mL) and 50 μL of phosphate buffer (500 mM, pH = 6) were mixed in a 1.5 mL plastic vial and further diluted to 300 μL with DI water. After the addition of 500 μL of Bradford reagent and incubation for 15 min, the UV−vis spectra were recorded.

Quantification of GOx in the Supernatant Using the Bradford Assay. 200 μL of supernatant, collected after the surfaces of CTAC-functionalized twinned cubes or as-obtained twinned cubes had been modified with GOx, was added into a 1.5 mL plastic vial, followed by the injection of 0−20 μL of GOx solutions (100 units/mL) and 50 μL of phosphate buffer (500 mM, pH = 6). The solution was further diluted to 300 μL with DI water, followed by the addition of 500 μL of Bradford reagent. After incubation for 15 min, the UV−vis spectra were recorded.

Etching of GOx-Functionalized Twinned Cubes. 1−15 μL of glucose solution (2%) and 20 μL of phosphate buffer (500 mM, pH 6) were mixed with 1.0 mL of the suspension of GOx-functionalized twinned cubes hosted in a 5 mL glass vial under magnetic stirring at 600 rpm. The etching was allowed to proceed for different periods of time up to 120 min.

Etching of GOx-Functionalized Twinned Cubes in the Presence of Ag^+. 0−20 μL of aqueous $AgNO_3$ (10 mM), 15 μL of glucose solution (2%), and 20 μL of phosphate buffer (500 mM, pH 6) were mixed with 1.0 mL of the suspension of GOx-functionalized twinned cubes hosted in a 5 mL glass vial under magnetic stirring at 600 rpm. The etching was allowed to proceed for different periods of time up to 120 min.

Etching of CTAC-Functionalized Twinned Cubes by H_2O_2. 1 mL of the suspension of CTAC-functionalized twinned cubes was added into a 5 mL glass vial, followed by the introduction of aqueous H_2O_2 with concentrations controlled in the range of 0.1 mM to 5 M under magnetic stirring at 600 rpm. The etching was allowed to proceed for different periods of time up to 60 min.

Preparation of GOx-Functionalized Ag Nanocubes. 0.01 mL of the as-prepared suspension of Ag nanocubes was added into an aqueous solution containing 0.1 mL of CTAC (10 mM) and 0.89 mL of DI water hosted in a 1 mL vial. After 30 min, the product was collected by centrifugation at 5000 rpm and then redispersed in 1.0 mL of DI water. In the second step, 1 mL of the CTAC-functionalized Ag nanocubes was added into a 5 mL glass vial, followed by the introduction of 10 μL of the GOx solutions (1000 units/mL) and incubation for 5 min.

Etching of the GOx-Functionalized Ag Nanocubes. 15 μL of glucose solution (2%) and 20 μL of phosphate buffer (500 mM, pH 6) were mixed with 1.0 mL of the GOx-functionalized Ag nanocubes hosted in a 5 mL glass vial under magnetic stirring at 600 rpm. The etching was allowed to proceed for different periods of time up to 120 min.

Instrumentation and Characterization. The UV−vis spectra were recorded using a Cary 60 spectrometer (Agilent Technologies, Santa Clara, CA). Dynamic light scattering (DLS) characterization was conducted with a Nano ZS Zetasizer (model ZEN3600, Malvern Instruments, Worcestershire, U.K.) using a He−Ne laser with a wavelength of 632.8 nm. An Eppendorf 5430 centrifuge was used for collecting and washing solid samples. Transmission electron microscopy (TEM) images were taken using a Hitachi HT7700 microscope (Hitachi, Tokyo, Japan) operated at 120 kV.

RESULTS AND DISCUSSION

Figure 1 outlines the three major steps involved in a typical experiment. The Ag twinned cubes bearing a negatively charged surface are first functionalized with cetyltrimethylammonium chloride (CTAC) to acquire some positive charges, followed by the immobilization of negatively charged GOx through electrostatic attraction to obtain GOx-functionalized twinned cubes. Using Bradford assay, we could quantify the amount of GOx adsorbed onto the surface of the twinned cubes. Upon the

DOI: 10.1021/acs.chemmater.6b03546
Chem. Mater. 2016, 28, 7519−7527

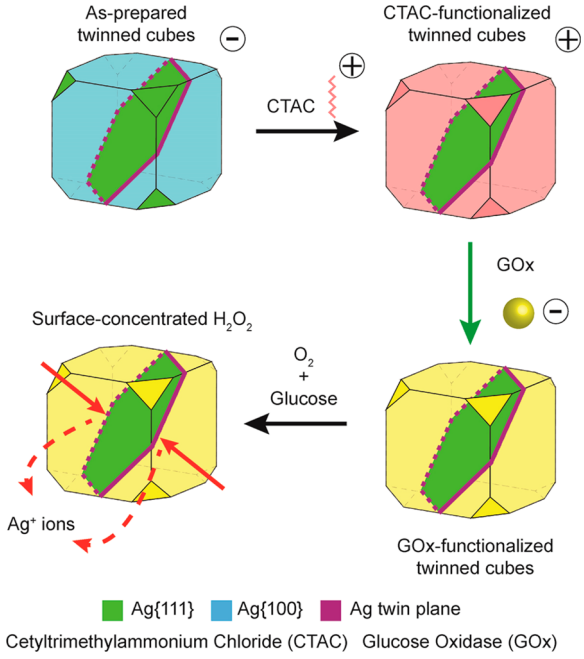

Figure 1. Schematic illustration of three major steps involved in an experiment: (i) modification of the as-prepared Ag twinned cubes with CTAC to switch the polarity of surface charges; (ii) functionalization of the CTAC-covered twinned cubes with GOx; and (iii) localized etching upon the introduction of glucose.

Table 1. Average Sizes and Zeta Potentials of As-Prepared Twinned Cubes, CTAC-Twinned Cubes, and Twinned Cubes Modified with Different Concentrations of GOx

sample	average size (nm)	zeta potential (mV)
as-prepared twinned cubes	46.1	−22.8
as-prepared twinned cubes + 5 units/mL GOx	47.1	−21.9
as-prepared twinned cubes + 10 units/mL GOx	48.8	−20.9
as-prepared twinned cubes + 20 units/mL GOx	51.9	−20.4
CTAC-functionalized twinned cubes	41.7	44.6
GOx-functionalized twinned cubes (5 units/mL)	53.3	22.9
GOx-functionalized twinned cubes (10 units/mL)	60.1	16.7
GOx-functionalized twinned cubes (20 units/mL)	155.9	14.6

introduction of glucose, H_2O_2 will be locally produced on the surface at a high concentration to initiate etching of Ag from the two {111} facets parallel to the twin plane.

We synthesized citrate-free Ag nanoplates and then used them as seeds for further growth to obtain Ag twinned cubes by following our previously reported protocols.[36,37] A typical growth process involved the introduction of 1 mL of $HAuCl_4$ (0.1 mM) into an aqueous suspension containing 100 μL of Ag nanoplates (0.37 mg/mL), 1 mL of ascorbic acid (AA, 100 mM), and 2 mL of poly(vinylpyrrolidone) (PVP, 1 mM), followed by the titration of aqueous $AgNO_3$ (2.0 mM) under ambient conditions. We used UV−vis spectroscopy to monitor the growth process (Figure S1A). Prior to the titration of any $AgNO_3$, we observed the formation of Ag−Au nanoframes (Figure S1B) due to the reduction of $HAuCl_4$ by Ag nanoplates and AA via galvanic replacement and reduction, respectively,

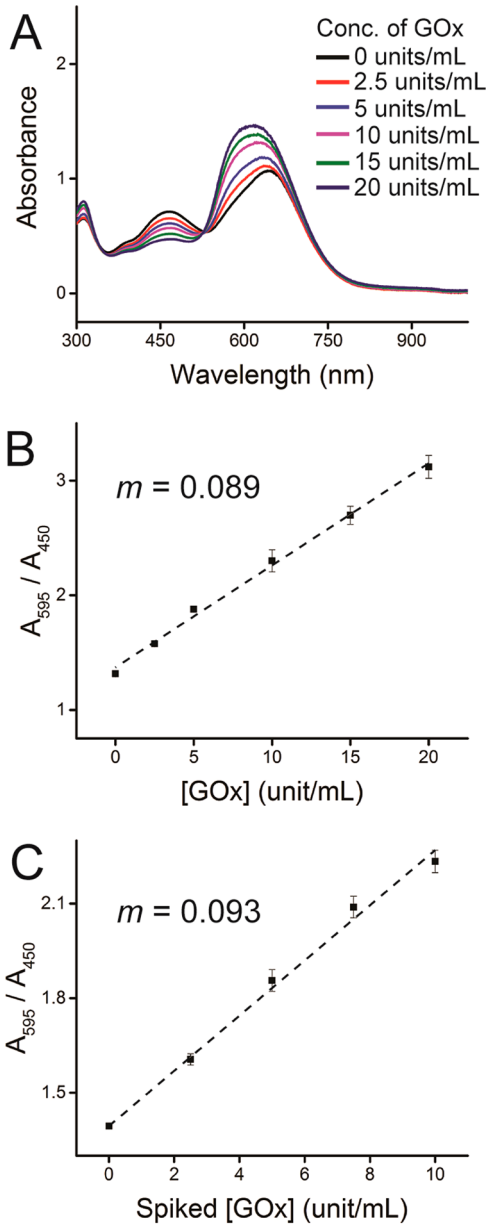

Figure 2. (A) UV−vis spectra recorded from Brilliant Blue G after reacting with GOx at different concentrations indicated on the curves. (B) Linear correlation between the ratio of absorbance of Brilliant Blue G at 595 and 450 nm (A_{595}/A_{450}) and the concentration of GOx. (C) Linear correlation between the ratio of absorbance of Brilliant Blue G at 595 and 450 nm (A_{595}/A_{450}) and the concentration of GOx spiked into the supernatant obtained after removal of the CTAC-functionalized twinned cubes.

and the deposition of Au. The Ag−Au nanoframes displayed a weak and broad LSPR peak between 700 and 800 nm. With the titration of $AgNO_3$ up to 0.1, 0.5, 0.8, and 1.5 mL, we noticed a constant blue shift for the LSPR peak from 624 to 436 nm (Figure S1A), indicating vertical growth for the Ag nanoplates.[35] Figure S1C−F shows TEM images of the resultant nanostructures at different titration volumes. At 1.5 mL, we obtained Ag twinned cubes with an average edge length of 47.3 ± 5.5 nm, together with some truncation at the corner sites. By considering that both $HAuCl_4$ and $AgNO_3$ would be reduced into atoms and then deposited onto Ag nanoplates, we calculated the mass ratio between Ag and Au of as-prepared

DOI: 10.1021/acs.chemmater.6b03546
Chem. Mater. 2016, 28, 7519−7527

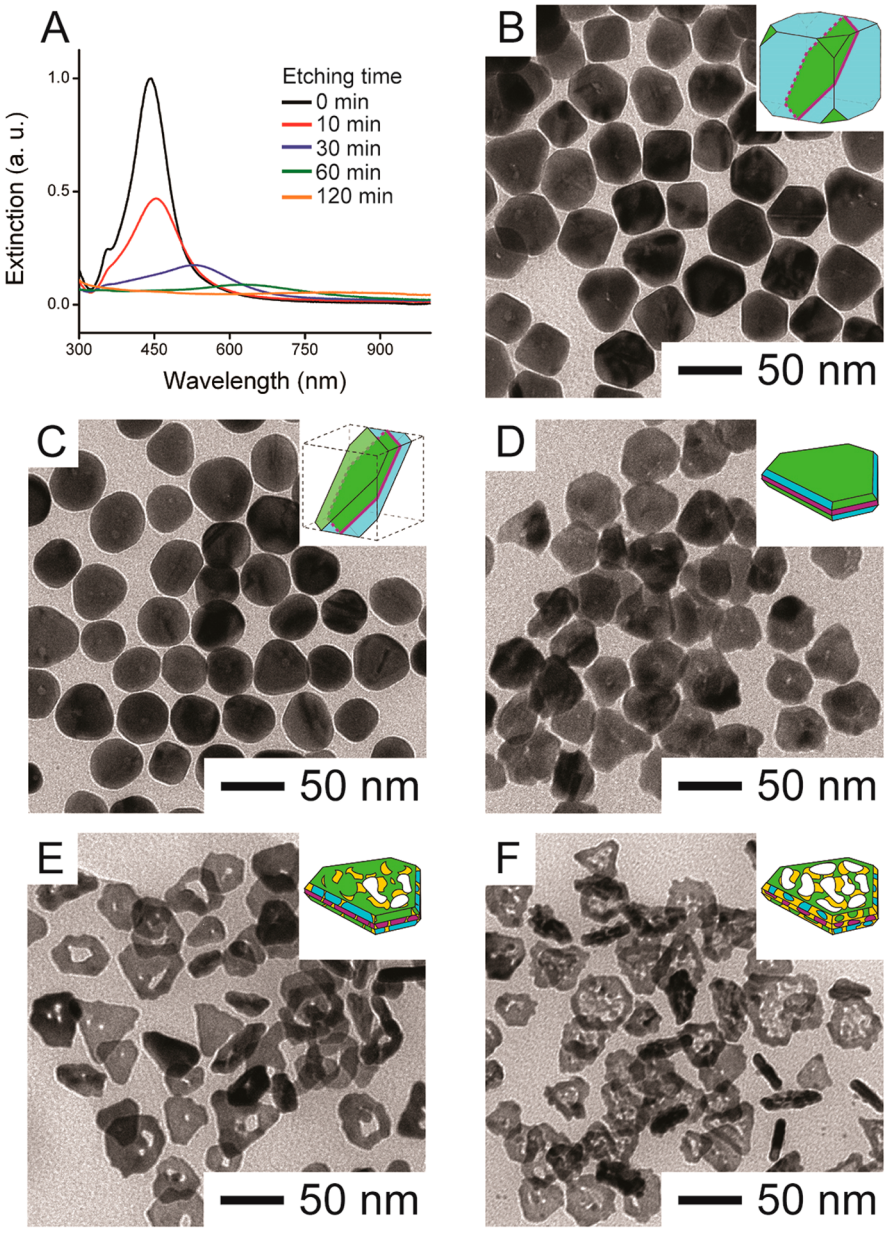

Figure 3. (A) UV−vis spectra collected at different time points indicated on the curves upon the introduction of glucose (2%, 15 μL) into a suspension of the GOx-functionalized twinned cubes in PBS buffer at pH = 6. (B−F) TEM images of the products of an etching experiment obtained (B) before and (C−F) after the introduction of glucose for 15, 30, 60, and 120 min, respectively.

twinned cubes to be 18.1:1. As shown in Table 1, the as-prepared twinned cubes were negatively charged.

It is critical for the surface of the nanoparticles to bear positive charges for the immobilization of negatively GOx through electrostatic attraction.[32] In practice, we applied CTAC modification to reserve the sign of surface charges. We used dynamic light scattering (DLS) to fully characterize the nanoparticles when their surfaces were functionalized with CTAC and/or GOx. When the Ag twinned cubes were functionalized with GOx only at concentrations of 5, 10, and 20 units/mL, we observed very little changes to both the hydrodynamic size and the zeta potential. In this case, the negatively charged GOx could not adsorb onto the twinned cubes via electrostatic attraction. In comparison, upon the treatment with CTAC, we noticed that the zeta potential was changed from −22.8 to 44.6 mV, confirming the formation of CTAC-functionalized twinned cubes covered by a positively charged surface. The hydrodynamic diameter slightly decreased from 46.1 to 41.7 nm. When these positively charged twinned cubes were incubated with GOx at concentrations of 5 and 10 units/mL, we observed the zeta potential decrease from 44.6 to 22.9 and 16.7, accompanied by an increase in hydrodynamic diameter from 41.7 to 53.3 and 60.1 nm, respectively. These data indicate the formation of GOx-functionalized twinned cubes. It should be pointed out that, when the concentration of GOx was further increased to 20 units/mL, the twinned cubes tended to aggregate with a significant increase in size up to 155.9 nm, primarily due to the neutralization of surface charges.

After incubation with GOx, we also used Bradford assay to determine the amount of GOx adsorbed on the surface of twinned cubes by measuring the concentration of GOx remaining in the supernatant. Bradford assay is a commonly

DOI: 10.1021/acs.chemmater.6b03546
Chem. Mater. 2016, 28, 7519−7527

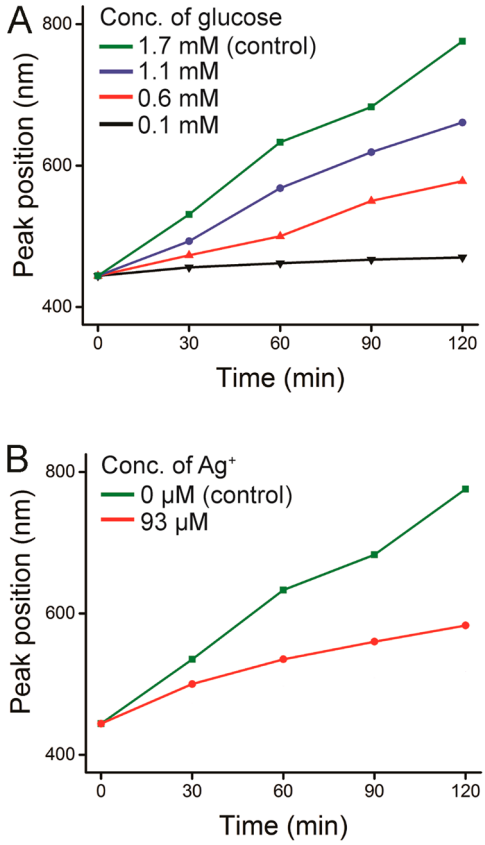

Figure 4. (A) The LSPR peak position of the GOx-functionalized twinned cubes at different time points upon the introduction of glucose at different final concentrations. (B) The LSPR peak position of the GOx-functionalized twinned cubes at different time points upon the introduction of glucose in the absence and presence of 93 μM $AgNO_3$, respectively. The final concentration of glucose was controlled at 1.7 mM for both samples.

used colorimetric method for measuring the concentration of proteins in a solution. In a typical measurement, UV−vis spectroscopy is used to record the absorption spectrum of Brilliant Blue G upon its binding to the nonpolar region and positively charged amine group on proteins via hydrophobic and electrostatic interactions, respectively.[39] Figure 2A shows the UV−vis spectra of Brilliant Blue G in a 31.3 mM phosphate buffer at pH = 6 after mixing with GOx at different concentrations. The two absorption peaks located at 595 and 450 nm could be assigned to the anionic and cationic forms of Brilliant Blue G, respectively. As the concentration of GOx was increased, the absorption peak at 595 nm increased in intensity while the peak at 450 nm decreased. Figure 2B shows a plot of the ratio between the absorbance at 595 and 450 nm (A_{595}/A_{450}) as a function of the GOx concentration in the range of 0−20 units/mL, indicating a linear progression with a slope of 0.089. We then used this method to determine the concentration of GOx remaining in the supernatant after incubation with the CTAC-functionalized twinned cubes. In this case, it is worth pointing out that the supernatant could possibly contain some CTAC that would help stabilize the anionic form of Brilliant Blue G and thus lead to a stronger response to GOx. Figure 2C shows the relationship between the ratio of A_{595}/A_{450} and the concentration GOx spiked into the supernatant from a suspension of the CATC-functionalized twinned cubes, showing a slope of 0.093, which was indeed slightly larger than 0.089. As a result, we should use the calibration curve shown in Figure 2C to measure the concentration of GOx remaining in the supernatant after incubation with the CTAC-functionalized twinned cubes. On the basis of the data from the Bradford assay, we found that the concentration of GOx remaining in the supernatant was 1.72 units/mL after incubation with the CTAC-functionalized twinned cubes at an initial concentration of 10 units/mL. In other words, 8.28 units/mL of GOx had been immobilized onto the surface of twinned cubes through electrostatic attraction.

We investigated the etching of the GOx-functionalized twinned cubes in a phosphate buffer by adding different amounts of a 2% glucose solution. We specifically chose phosphate buffer with a pH at 6.0 to achieve the optimal condition for GOx activity.[34] In a typical experiment, we functionalized the twinned cubes with CTAC, followed by modification with GOx at a concentration of 10 units/mL for 5 min. The UV−vis spectra recorded from the twinned cubes after the two modification steps (Figure S2) were essentially identical to that of the as-prepared twinned cubes. This result confirms the preservation of size, shape, and morphology during the entire surface modification process. Next, we added 15 μL of glucose solution (1.7 mM) into the suspension of nanoparticles to initiate etching, and then monitored the progress by collecting UV−vis spectra at different time points (Figure 3A). The LSPR peak showed a marked decrease in intensity just after 10 min, together with a red shift from 443 to 452 nm. As the etching time was increased to 30, 60, and 120 min, the peak was further red-shifted to 530, 633, and 776 nm, together with significant drop in intensity. Figure 3B−F shows TEM images of the resultant nanostructures at different stages of the etching process. These images suggest that the etching was preferentially initiated from the Ag atoms located at the two {111} facets parallel to the twin plane and progressed through the sequential removal of {111} planes for the transformation of a twinned cube into a nanoplate and then a Ag−Au nanoframe. By comparing with the results obtained from the vertical growth of Ag nanoplates into twinned cubes (Figure S1), it is evident that the etching process followed exactly the same pathway of a growth process, except for the reversed sequence.[35]

To confirm the role of GOx on the surfaces of twinned cubes in accelerating the etching process, we performed a control experiment by mixing the as-prepared twinned cubes with GOx, followed by the addition of glucose. Again, we conducted the Bradford assay to determine the concentration of GOx remaining in the supernatant. Figure S3 shows the relationship between the ratio of A_{595}/A_{450} and the concentration GOx spiked into the supernatant from a suspension of the as-prepared twinned cubes. The result indicates that the concentration of GOx remaining in the supernatant was 9.89 units/mL, suggesting 0.11 units/mL of GOx had been adsorbed onto the surface of twinned cubes. Upon the addition of glucose to the mixture of as-prepared twinned cubes and GOx, Figure S4 shows that the LSPR peak was shifted from 433 to 786 nm after 360 min, indicating that the etching process was much slower than that of GOx-functionalized twinned cubes (see Figure 3A).

We performed another set of experiments by varying the incubation time with GOx from 5 min to 30, 60, and 180 min, respectively. As shown in Figure S5A, the UV−vis spectra recorded from the resultant twinned cubes showed very little change upon surface modification with GOx for different

DOI: 10.1021/acs.chemmater.6b03546
Chem. Mater. 2016, 28, 7519−7527

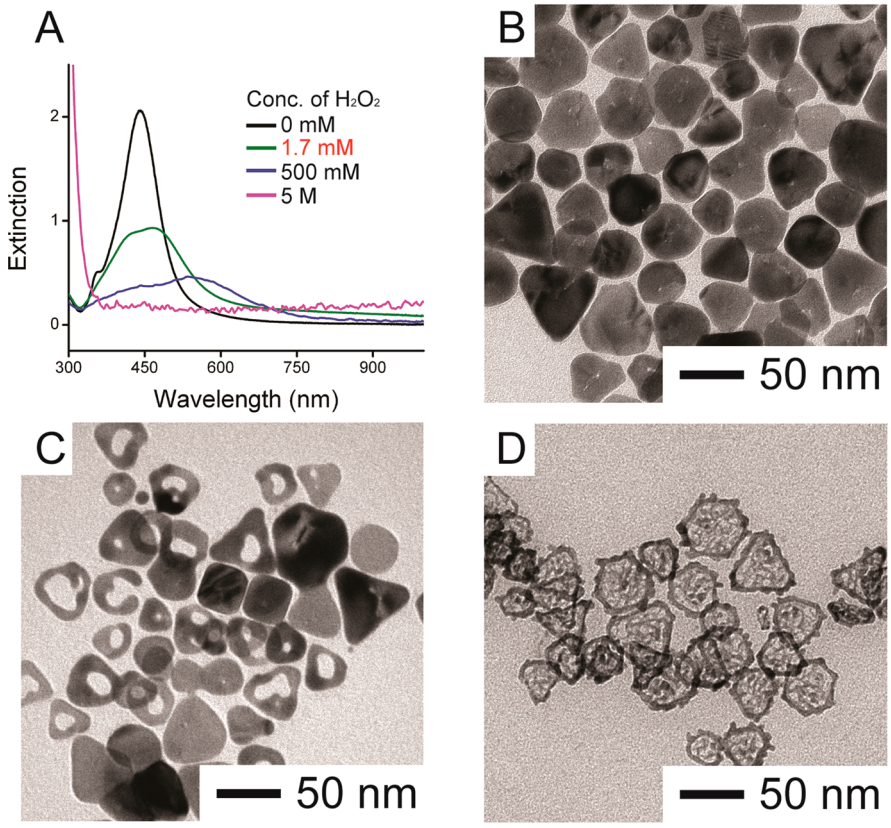

Figure 5. (A) UV−vis spectra of the products obtained by reacting the GOx-functionalized twinned cubes with H_2O_2 at different concentrations indicated on the curves for 60 min. (B−D) TEM images of the corresponding products obtained after etching with H_2O_2 at different concentrations.

periods of time. For each sample, upon the introduction of glucose at a concentration of 1.7 mM, we collected a series of UV−vis spectra at different time points up to 120 min. Figure S5B shows a plot of the LSPR peak position as a function of time, indicating that the GOx-functionalized twinned cubes prepared with different incubation times were almost identical to the twinned cubes obtained with an incubation time of 5 min. Collectively, our data suggest that the GOx-functionalized twinned cubes were stable in a phosphate buffer and the GOx could adsorb onto the CTAC-functionalized surface within 5 min.

To understand the role of glucose in controlling the etching process, we performed a set of experiments by adding different amounts of glucose into the same amount of an aqueous suspension of GOx-functionalized twinned cubes. At each concentration of glucose, we collected a series of UV−vis spectra at different time points up to 120 min post the introduction of glucose. Figure 4A shows a plot of the LSPR peak position as a function of the etching time. At 0.1 mM glucose, we only observed minor shifts for the LSPR peak position from 443 to 470 nm, indicating an ineffective etching process. When the glucose concentration was increased to 0.6, 1.1, or 1.7 mM, we observed red shifts for the LSPR peak from 443 to 578, 661, and 776 nm, respectively, at an etching time of 120 min. These results indicate that the etching would become faster at a higher concentration of glucose due to an increase in the local concentration of H_2O_2 on the surface of twinned cubes.

It is well-known that the Ag^+ ions could inhibit the activity of GOx.[40] The Ag^+ ions could also possibly shift the chemical equilibrium for the oxidation reaction of Ag backward and thus suppress the etching. By assuming that the etching of Ag twinned cubes would proceed along the reversed pathway for the growth of nanoplates, the concentration of Ag^+ could reach a level of 93 μM after the twinned cubes had been etched into the plates shown in Figure 3C according to the amount of $AgNO_3$ required for the transformation of the plates into twinned cubes during growth (Figure S1E,F). Figure 4B compares the changes to the LSPR peak position as a function of etching time in the absence and presence of $AgNO_3$, respectively. At an etching time of 120 min, the peak position was only red-shifted from 443 to 583 nm in the presence of 93 μM $AgNO_3$. This result confirms that the etching would be slowed down as more Ag atoms were oxidized and released as Ag^+ ions into the reaction solution.

We compared the etching of GOx-functionalized twinned cubes by glucose with that of CTAC-functionalized twinned cubes using directly added aqueous H_2O_2. Figure 5A shows the UV−vis spectra of CTAC-functionalized twinned cubes that were collected after reacting with aqueous H_2O_2 at different concentrations for 60 min. At a concentration of 1.7 mM, equivalent to what was produced by enzymatic oxidation of glucose, we noticed that the LSPR peak of the twinned cubes was largely retained in peak position, only showing intensity drop and peak broadening. The TEM images recorded from resultant nanostructures indicate the formation of a mixture of twinned cubes, thick plates, and thin plates (Figure 5B). These results are completely different from what was observed in the etching of GOx-functionalized twinned cubes by glucose. In the latter case, at an etching time of 60 min, the LSPR peak was shifted to 663 nm and Ag−Au nanoframes were formed (Figure 3A,E). In an aqueous solution, the added H_2O_2 would

DOI: 10.1021/acs.chemmater.6b03546
Chem. Mater. 2016, 28, 7519−7527

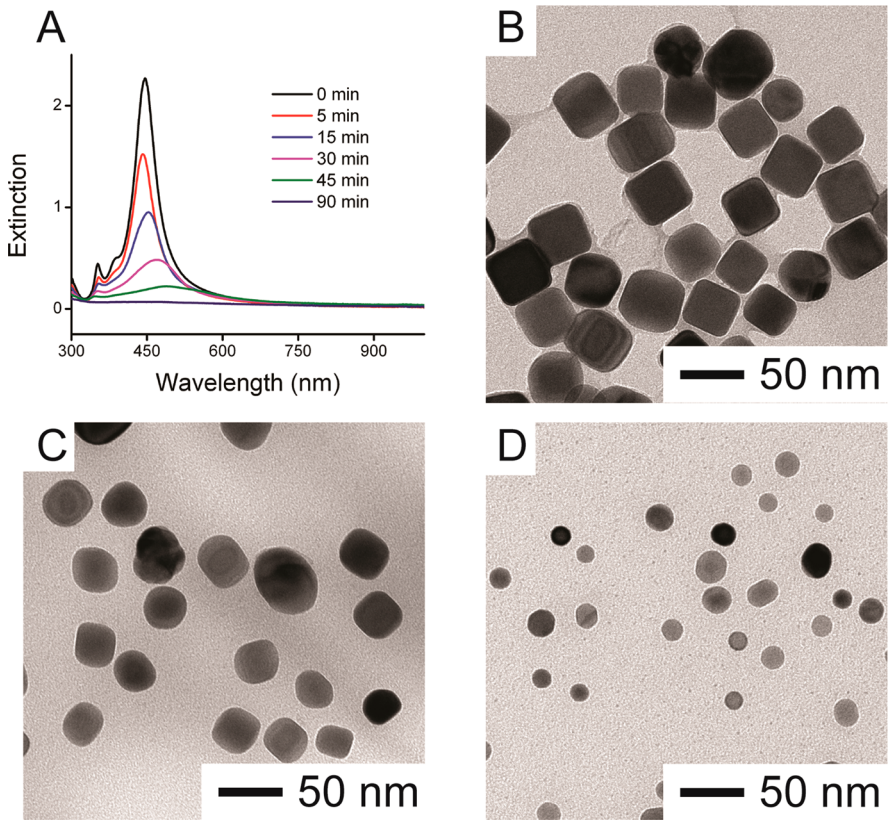

Figure 6. (A) UV−vis spectra obtained from the products after mixing glucose with the GOx-functionalized cubes for different periods of time indicated on the curves. (B−D) TEM images of the products obtained by reacting the GOx-functionalized cubes with glucose for (B) 0, (C) 15, and (D) 45 min, respectively.

spontaneously decompose to H_2O and O_2, making the etching less effective. When the concentration of aqueous H_2O_2 was increased to 500 mM, we observed a red shift of the LSPR peak to 565 nm and the formation of structures that include thin plates, Ag−Au nanoframes, and twinned cubes (Figure 5C). In this case, we suspect that the directly added H_2O_2 molecules could reach the surface of a twinned cube via diffusion. Different twinned cubes would be exposed to H_2O_2 at different local concentrations, leading to the formation of diverse structures from the twinned cubes. With a further increase of H_2O_2 concentration to 5M, we finally observed the formation of Ag−Au nanoframes (Figure 5D) similar to the products obtained by etching the GOx-functionalized twinned cubes with glucose (Figure 3F).

We also examined the etching of conventional, single-crystal Ag cubes after GOx functionalization by following all the procedures described in the standard protocol except for the replacement of Ag twinned cubes with single-crystal cubes.[38] Figure 6A shows the UV−vis spectra of Ag nanocubes collected at different time points up to 90 min after the addition of glucose. We observed a gradual decrease in intensity for the LSPR peak at 441 nm as the etching proceeded. The LSPR peak disappeared at 90 min, indicating the complete dissolution of the Ag nanocubes. The TEM images in Figure 6B−D indicate the transformation of the Ag cubes into rounded cubes and then spherical particles. In this case, unlike the Ag twinned cubes, the etching would be initiated from the corners and edges of a Ag cube, leading to its gradual transformation into a spherical particle.

CONCLUSIONS

In summary, we have demonstrated that the surface-concentrated H_2O_2 derived from the enzymatic oxidation of glucose could accelerate the etching of Ag nanocrystals with selectivity. In the case of Ag twinned cubes, we observed that the etching would begin from the Ag atoms located at the two {111} facets parallel to the twinned plane, followed by the sequential removal of {111} planes, leading to the transformation of twinned cubes into Ag nanoplates in the order opposite to the growth process. An increase in the concentration of glucose would accelerate the etching process because of the production of more H_2O_2 at the expense of glucose. On the other hand, we noticed that the dissolved Ag^+ ions from twinned cubes could potentially deactivate GOx and thus decrease the production of H_2O_2 and slow down the etching. When benchmarked against etching with the direct introduction of aqueous H_2O_2, we found that 1.7 mM enzymatic H_2O_2 (from glucose) was equivalent to 5 M aqueous H_2O_2 in terms of etching rate and outcome. Our results suggest that the enzymatic oxidation of glucose could serve as a useful platform for generating highly concentrated H_2O_2 on the surface of nanoparticles for their etching in a more controllable fashion to maneuver their size, shape, and morphology for a variety of applications.

ASSOCIATED CONTENT

Supporting Information

The Supporting Information is available free of charge on the ACS Publications website at DOI: 10.1021/acs.chemmater.6b03546.

DOI: 10.1021/acs.chemmater.6b03546
Chem. Mater. 2016, 28, 7519−7527

SEM, TEM images, and UV−vis spectra (PDF)

AUTHOR INFORMATION

Corresponding Author

*E-mail: dong.qin@mse.gatech.edu.

Notes

The authors declare no competing financial interest.

ACKNOWLEDGMENTS

This work was supported in part by the National Science Foundation (CHE-1412006), start-up funds from Georgia Tech, and a 3M nontenured faculty award. Part of the work was performed in the Institute of Electronics and Nanotechnology (IEN) at the Georgia Institute of Technology. C.-W.W. was also partially supported by the graduate student study abroad program from the Ministry of Science and Technology (MOST) in Taiwan (MOST-104-2917-I-002-015).

REFERENCES

(1) Jain, P. K.; Huang, X.; El-Sayed, I. H.; El-Sayed, M. A. Noble Metals on the Nanoscale: Optical and Photothermal Properties and Some Applications in Imaging, Sensing, Biology, and Medicine. *Acc. Chem. Res.* **2008**, *41*, 1578−1586.

(2) Haes, A. J.; Haynes, C. L.; McFarland, A. D.; Schatz, G. C.; Van Duyne, R. P.; Zou, S. Plasmonic Materials for Surface-Enhanced Sensing and Spectroscopy. *MRS Bull.* **2005**, *30*, 368−375.

(3) Willets, K. A.; Van Duyne, R. P. Localized Surface Plasmon Resonance Spectroscopy and Sensing. *Annu. Rev. Phys. Chem.* **2007**, *58*, 267−297.

(4) Xia, Y.; Li, W.; Cobley, C. M.; Chen, J.; Xia, X.; Zhang, Q.; Yang, M.; Cho, E. C.; Brown, P. K. Gold nanocages: From Synthesis to Theranostic Applications. *Acc. Chem. Res.* **2011**, *44*, 914−924.

(5) Rosi, N. L.; Mirkin, C. A. Nanostructures in Biodiagnostics. *Chem. Rev.* **2005**, *105*, 1547−1562.

(6) Qian, X.; Peng, X.-H.; Ansari, D. O.; Yin-Goen, Q.; Chen, G. Z.; Shin, D. M.; Yang, L.; Young, A. N.; Wang, M. D.; Nie, S. In Vivo Tumor Targeting and Spectroscopic Detection with Surface-Enhanced Raman Nanoparticle Tags. *Nat. Biotechnol.* **2008**, *26*, 83−90.

(7) Lal, S.; Clare, S. E.; Halas, N. J. Nanoshell-enabled Photothermal Cancer Therapy: Impending Clinical Impact. *Acc. Chem. Res.* **2008**, *41*, 1842−1851.

(8) Burda, C.; Chen, X.; Narayanan, R.; El-Sayed, M. A. Chemistry and Properties of Nanocrystals of Different Shapes. *Chem. Rev.* **2005**, *105*, 1025−1102.

(9) Zhang, H.; Jin, M.; Xia, Y. Enhancing the Catalytic and Electrocatalytic Properties of Pt-based Catalysts by Forming Bimetallic Nanocrystals with Pd. *Chem. Soc. Rev.* **2012**, *41*, 8035−8049.

(10) Joo, S. H.; Park, J. Y.; Tsung, C.-K.; Yamada, Y.; Yang, P.; Somorjai, G. A. Thermally stable Pt/mesoporous silica core-shell nanocatalysts for high-temperature reactions. *Nat. Mater.* **2009**, *8*, 126−131.

(11) Zhang, Z.; Luo, Z.; Chen, B.; Wei, C.; Zhao, J.; Chen, J.; Zhang, X.; Lai, Z.; Fan, Z.; Tan, C.; Zhao, M.; Lu, Q.; Li, B.; Zong, Y.; Yan, C.; Wang, G.; Xu, Z. J.; Zhang, H. One-Pot Synthesis of Highly Anisotropic Five-Fold-Twinned PtCu Nanoframes Used as a Bifunctional Electrocatalyst for Oxygen Reduction and Methanol Oxidation. *Adv. Mater.* **2016**, DOI: 10.1002/adma.201603075.

(12) Fan, Z.; Luo, Z.; Huang, X.; Li, B.; Chen, Y.; Wang, J.; Hu, Y.; Zhang, H. Synthesis of 4H/fcc Noble Multimetallic Nanoribbons for Electrocatalytic Hydrogen Evolution Reaction. *J. Am. Chem. Soc.* **2016**, *138*, 1414−1419.

(13) Jana, N. R.; Gearheart, L.; Murphy, C. J. Wet Chemical Synthesis of High Aspect Ratio Cylindrical Gold Nanorods. *J. Phys. Chem. B* **2001**, *105*, 4065−4067.

(14) Sun, Y.; Gates, B.; Mayers, B.; Xia, Y. Crystalline Silver Nanowires by Soft Solution Processing. *Nano Lett.* **2002**, *2*, 165−168.

(15) Xia, Y.; Xiong, Y.; Lim, B.; Skrabalak, S. E. Shape-controlled synthesis of metal nanocrystals: simple chemistry meets complex physics? *Angew. Chem., Int. Ed.* **2009**, *48*, 60−104.

(16) Tao, A. R.; Habas, S.; Yang, P. Shape Control of Colloidal Metal Nanocrystals. *Small* **2008**, *4*, 310−325.

(17) Cobley, C. M.; Rycenga, M.; Zhou, F.; Li, Z.-Y.; Xia, Y. Etching and Growth: an Intertwined Pathway to Silver Nanocrystals with Exotic Shapes. *Angew. Chem., Int. Ed.* **2009**, *48*, 4824−4827.

(18) Mulvihill, M. J.; Ling, X. Y.; Henzie, J.; Yang, P. Anisotropic Etching of Silver Nanoparticles for Plasmonic Structures Capable of Single-particle SERS. *J. Am. Chem. Soc.* **2010**, *132*, 268−274.

(19) Liu, M.; Zheng, Y.; Zhang, L.; Guo, L.; Xia, Y. Transformation of Pd Nanocubes into Octahedra with Controlled Sizes by Maneuvering the Rates of Etching and Regrowth. *J. Am. Chem. Soc.* **2013**, *135*, 11752−11755.

(20) Yang, Y.; Zhong, X.-L.; Zhang, Q.; Blackstad, L. G.; Fu, Z.; Li, Z.-Y.; Qin, D. The Role of Etching in the Formation of Ag Nanoplates with Straight, Curved and Wavy Edges and Comparison of Their SERS Properties. *Small* **2014**, *10*, 1430−1437.

(21) Wang, Z.; Yang, G.; Zhang, Z.; Jin, M.; Yin, Y. Selectivity on Etching: Creation of High-Energy Facets on Copper Nanocrystals for CO_2 Electrochemical Reduction. *ACS Nano* **2016**, *10*, 4559−4564.

(22) Rycenga, M.; Cobley, C. M.; Zeng, J.; Li, W.; Moran, C. H.; Zhang, Q.; Qin, D.; Xia, Y. Controlling the Synthesis and Assembly of Silver Nanostructures for Plasmonic Applications. *Chem. Rev.* **2011**, *111*, 3669−3712.

(23) Zhang, Q.; Cobley, C. M.; Zeng, J.; Wen, L.-P.; Chen, J.; Xia, Y. Dissolving Ag from Au−Ag Alloy Nanoboxes with H_2O_2: A Method for Both Tailoring the Optical Properties and Measuring the H_2O_2 Concentration. *J. Phys. Chem. C* **2010**, *114*, 6396−6400.

(24) Yang, Y.; Zhang, Q.; Fu, Z.; Qin, D. Transformation of Ag Nanocubes into Ag-Au Hollow Nanostructures with Enriched Ag Contents to Improve SERS Activity and Chemical Stability. *ACS Appl. Mater. Interfaces* **2014**, *6*, 3750−3757.

(25) Sun, X.; Qin, D. Co-titration of $AgNO_3$ and $HAuCl_4$: A New Route to the Synthesis of Ag@Ag−Au Core−Frame Nanocubes with Enhanced Plasmonic and Catalytic Properties. *J. Mater. Chem. C* **2015**, *3*, 11833−11841.

(26) Li, J.; Sun, X.; Qin, D. Ag-Enriched Ag-Pd Bimetallic Nanoframes and Their Catalytic Properties. *ChemNanoMat* **2016**, *2*, 494−499.

(27) Sun, X.; Kim, J.; Gilroy, K. D.; Liu, J.; Konig, T. A. F.; Qin, D. Gold-Based Cubic Nanoboxes with Well-Defined Openings at the Corners and Ultrathin Walls Less Than Two Nanometers Thick. *ACS Nano* **2016**, *10*, 8019−8025.

(28) Wu, H.; Wang, P.; He, H.; Jin, Y. Controlled Synthesis of Porous Ag/Au Bimetallic Hollow Nanoshells with Tunable Plasmonic and Catalytic Properties. *Nano Res.* **2012**, *5*, 135−144.

(29) McEachran, M.; Keogh, D.; Pietrobon, B.; Cathcart, N.; Gourevich, I.; Coombs, N.; Kitaev, V. Ultrathin Gold Nanoframes Through Surfactant-Free Templating of Faceted Pentagonal Silver Nanoparticles. *J. Am. Chem. Soc.* **2011**, *133*, 8066−8069.

(30) Wilson, R.; Turner, A. P. F Glucose Oxidase: An Ideal Enzyme. *Biosens. Bioelectron.* **1992**, *7*, 165−185.

(31) Wang, J. Electrochemical Glucose Biosensors. *Chem. Rev.* **2008**, *108*, 814−825.

(32) Steiner, M.-S.; Duerkop, A.; Wolfbeis, O. S. Optical Methods for Sensing Glucose. *Chem. Soc. Rev.* **2011**, *40*, 4805−4839.

(33) He, H.; Xu, X.; Wu, H.; Jin, Y. Enzymatic Plasmonic Engineering of Ag/Au Bimetallic Nanoshells and Their Use for Sensitive Optical Glucose Sensing. *Adv. Mater.* **2012**, *24*, 1736−1740.

(34) He, H.; Xu, X.; Wu, H.; Zhai, Y.; Jin, Y. In Situ Nanoplasmonic Probing of Enzymatic Activity of Monolayer-Confined Glucose Oxidase on Colloidal Nanoparticles. *Anal. Chem.* **2013**, *85*, 4546−4553.

(35) Xia, Y.; Ye, J.; Tan, K.; Wang, J.; Yang, G. Colorimetric visualization of glucose at the submicromole level in serum by a homogenous silver nanoprism-glucose oxidase system. *Anal. Chem.* **2013**, *85*, 6241−6247.

DOI: 10.1021/acs.chemmater.6b03546
Chem. Mater. 2016, 28, 7519−7527

(36) Zhang, Q.; Yang, Y.; Li, J.; Iurilli, R.; Xie, S.; Qin, D. Citrate-free Synthesis of Silver Nanoplates and the Mechanistic Study. *ACS Appl. Mater. Interfaces* **2013**, *5*, 6333−6345.
(37) Zhang, J.; Liu, J.; Xie, Z.-X.; Qin, D. $HAuCl_4$: A Dual Agent for Studying the Chloride-Assisted Vertical Growth of Citrate-Free Ag Nanoplates with Au Serving as a Marker. *Langmuir* **2014**, *30*, 15520−15530.
(38) Zhang, Q.; Li, W.; Wen, L. P.; Chen, J.; Xia, Y. Facile Synthesis of Ag Nanocubes of 30 to 70 nm in Edge Length with CF_3COOAg as a Precursor. *Chem.—Eur. J.* **2010**, *16*, 10234−10239.
(39) Zor, T.; Selinger, Z. Linearization of the Bradford Protein Assay Increases its Sensitivity: Theoretical and Experimental Studies. *Anal. Biochem.* **1996**, *236*, 302−308.
(40) Copeland, R. A.; Fodor, S. P. A.; Spiro, T. G. Surface-Enhanced Raman Spectra of an Active Flavo Enzyme: Glocose Oxidase and Riboflavin Binding Protein on Silver Particles. *J. Am. Chem. Soc.* **1984**, *106*, 3872−3874.

DOI: 10.1021/acs.chemmater.6b03546
Chem. Mater. 2016, 28, 7519−7527